Chapter 5

Selection in System and Sensor

W. Olthuis, S. Böhm, G. R. Langereis and P. Bergveld

MESA+ Research Institute, University of Twente, P.O. Box 217, 7500 AE Enschede, The Netherlands

Since the dawn of chemical sensors, there were high hopes of rapid and widespread utilization of these devices. This predicted success, however, has not yet been achieved, due to several causes: (bio)chemical fouling of the sensor, instability in the sensor signal resulting in drift, and lack of available selector materials, specific for all species to be detected.
In this chapter, a more realistic approach is pursued, i.e., the incorporation of the sensing element in a Total Analysis System (TAS). This system comprises a double-lumen microdialysis probe, providing a coarse first-stage selection of molecules, to be allowed into the system, decreasing the possibility of sensor fouling. Additionally, the system is provided with integrated electrochemically driven pumps to precisely dose nanoliter amounts of calibration liquid, for periodic calibration of the possibly drifting sensing element.
A possible and simple sensing element in these kind of TAS's is a conductivity probe. Electrolyte Conductivity (EC) is not selective for specific ions. It is shown in this chapter, however, that separate ion concentrations can be calculated, when the EC is measured at several temperatures, using the characteristic temperature responses of the ionic conductivities of these ions.

Selection with a Total Analysis System (TAS)

General

An ideal chemical sensor would transfer concentration information of a specific chemical compound with 100 per cent selectivity, i.e., without any cross-sensitivity to the electrical (or optical) domain. Additionally, such a sensor must be able to operate directly in the sample solution. Schematically, such a sensor is shown in Figure 1.

Despite all efforts, such sensors do not exist. Nevertheless, with full scale laboratory equipment, analysts are often able, off-line, to specifically characterize a certain sample after laborious sample pre-treatment. The development of a TAS is an attempt to integrate component-wise the several relevant sub-systems involved in laboratory equipment on a small scale. The functions these components should fulfill are typically sampling, transport, mixing, reaction, separation and detection. If this TAS is very close to the place of the actual measurement, then the system is commonly referred to as micro- or μ-TAS *(1)*. An impression of such a μ-TAS, showing some of the relevant sub-systems, is given in Figure 2. It is beyond the scope of this chapter to describe all the possible advantages of μ-TAS, already partly realized and described in, e.g., *(2)*.

In this section, we restrict ourselves to two problems, related to the direct use of chemical sensors, i.e., (bio)chemical fouling and instability of the sensor signal, which can to a certain extent be solved by using a TAS, as shown in the next sub-sections.

Microdialysis probe

A realistic approach to the problem of fouling of the sensor surface, especially by large, solid particles and proteins is by separating these interfering compounds from the chemical sensor. Precisely this is accomplished by the microdialysis technique *(3)*. A perfusion liquid is pumped through a hollow fiber, in contact with the sample solution to be investigated. A part of this fiber consists of a semi-permeable membrane, such as cellulose acetate. During the passage of the perfusion liquid through the fiber, only substances of small molecular weight can diffuse through the membrane, preventing the fouling substances from entering the system. Subsequent analysis of the dialysate and detection of the species of interest is carried out off-site, but on-line in the TAS on a semi-continuous base. This system is schematically shown in Figure 3.

There are many parameters determining how well the concentration of the analyte in the dialysate agrees with that in the sample solution. This property is expressed by the relative recovery ratio R:

$$R = \frac{[analyte]_{dialysate}}{[analyte]_{sample}} * 100\% \qquad (1)$$

As can be imagined, R depends on the diffusion coefficient of the entering analyte, the residence time of the perfusate in the semi-permeable part of the lumen, and thus of the volumetric flow rate, and on dimensional parameters, like the length and radius of the semi-permeable part of the lumen.

Now let us calculate how long the perfusate should minimally stay in the semi-permeable part of the lumen in order to obtain a high R-value of, say, 90%. For this, flow is considered to be absent, and the length of the semi-permeable part of the lumen is considered to be much longer than its diameter. Mass transport is now

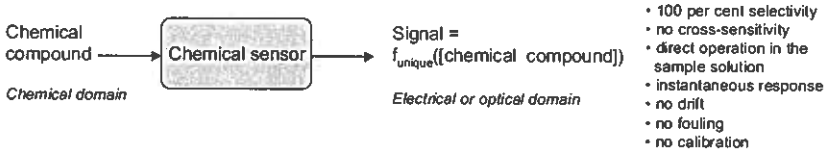

Figure 1. The ideal chemical sensor visualized; its function and its requirements.

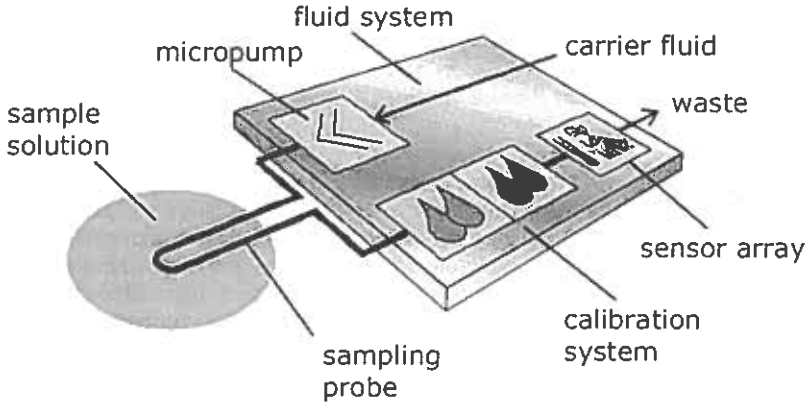

Figure 2. Impression of a Micro Total Analysis System showing several required sub-systems.

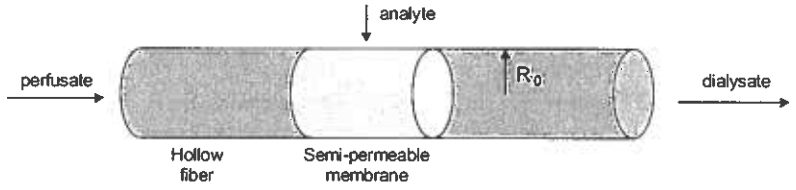

Figure 3. Illustration of the microdialysis technique, showing the hollow lumen of which a part consists of a semi-permeable membrane through which the analyte can enter the system.

governed by diffusion only. Of course, mass transport takes place from the semi-permeable membrane to the inner volume of the lumen. This process is described by the differential equation for diffusive mass transport in cylindrical co-ordinates:

$$\frac{\partial C}{\partial t} = \frac{D}{r}\cdot\frac{\partial}{r}\left(r\frac{\partial C}{\partial r}\right) = D\left(\frac{\partial^2 C}{\partial r^2}+\frac{1}{r}\frac{\partial C}{\partial r}\right), \qquad 0<r<R_0 \tag{2}$$

C and D being the concentration of the analyte in the lumen, and its diffusion coefficient, respectively. R_0 is the radius of the lumen, as also shown in Figure 3. At the start, we consider no analyte to be present in the lumen, and the semi-permeable membrane itself does not form an extra obstacle for diffusive transport. Then, the initial and boundary conditions become

$C=0 \quad 0<r<R_0 \quad t=0$ (3a)

$C=C_0 \quad r=R_0 \quad t\geq 0$ (3b)

with C_0 the concentration of the analyte in the sample. This concentration is considered to remain constant, due to a commonly relatively large sample volume and the presence of convection outside the lumen. Then the solution of the occurring concentration profile within the lumen, using eqns. 2, 3a and b is *(4)*

$$C(r,t) = C_0 - 2C_0\sum_{n=1}^{\infty} e^{-Dt\frac{\beta_n^2}{R_0^2}}\cdot\frac{J_0\left(\frac{r}{R_0}\beta_n\right)}{\beta_n J_1(\beta_n)} \tag{4}$$

with J_0 and J_1 the Bessel function of the first kind and order 0 and 1, respectively, and with β_n the roots of $J_0(\beta)=0$. For a worst case estimation, the longest distance to be traversed for the analyte is considered: from the wall to the center of the lumen, being the lumen radius, R_0. There, at $r=0$, the concentration is at its lowest. The expression for the concentration at $r=0$, relative to the analyte concentration in the sample, C_0, considering that $J_0(0)=1$, becomes

$$\frac{C(r=0,\tau)}{C_0} = 1 - 2\sum_{n=1}^{\infty} e^{-\beta_n^2\tau}\cdot\frac{1}{\beta_n J_1(\beta_n)} \tag{5}$$

introducing the dimensionless variable

$$\tau = \frac{Dt}{R_0^2} \tag{6}$$

A plot of $C(r=0, \tau)/C_0$ as a function of τ is shown in Figure 4a. A practical example is shown in Figure 4b, for a lumen radius $R_0=150\ \mu m$ and diffusion coefficient $D=1\cdot10^{-9}\ m^2/s$. It can be seen, that it takes ca. 11 s to reach 90% of the original sample concentration at the axis of the lumen, $r=0$.

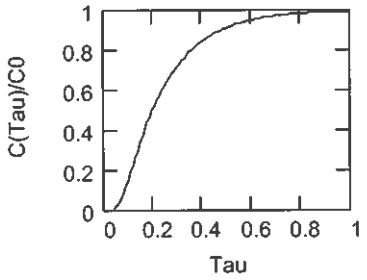

Figure 4a. Graph of the normalized concentration due to cylindrical diffusion as a function of the dimensionless variable, τ.

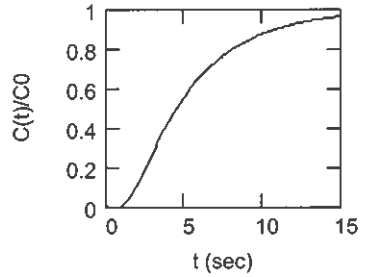

Figure 4b. Graph of the normalized concentration due to cylindrical diffusion as a function of time, t, for $D=1\cdot10^{-9}$ m^2/s and $R_0=150$ μm.

A more realistic and milder approach is to calculate the mean concentration of the sample in the lumen, averaged over its cross section *(4)*:

$$\frac{C_{mean}(\tau)}{C_0} = \frac{1}{\pi R_0^2}\int_{\varphi=0}^{2\pi}\int_{r=0}^{R_0}\frac{C(r,\tau)}{C_0}rdrd\varphi$$

$$= 1 - 4\sum_{n=1}^{\infty}\frac{e^{-\beta_n\tau}}{\beta_n^2} \qquad (7)$$

Also for this case, plots of this normalized mean concentration both as a function of the dimensionless variable τ and, as an example, as a function of time for $D=1\cdot10^{-9}$ m^2/s and $R_0=150$ μm is shown in Figure 5a and b, respectively. Now, already after ca. 7.5 s 90% of the original sample concentration is reached.

With this, the minimum residence time of the perfusate in the semi-permeable part of the lumen is estimated. Of course, due to convection, the non-zero distance between plug-formation of the dialysate and the detector, and the position of the sensing part of the detector itself, this calculated minimum residence time only forms a lower limit of the total sampling time of the probe. Precise calculations of these additional effects are beyond the framework of this chapter.

Microdialysis as a sampling tool for a μ-TAS is even more favourable, when a double-lumen microdialysis probe is used *(5, 6)*. Now, the perfusate is driven through a small inner tube, located within an outer tube. The fluid leaves the inner tube at the probe-tip and subsequently flows past the semi-permeable membrane back via the outer tube as schematically shown in Figure 6.

For an optimized design of the probe, it is important to know, that *R* is inversely proportional to the volumetric flow rate of the perfusate. In order to obtain a *R*-value near 100 per cent, which is favourable, because calibration of the probe is then not necessary, the flow rate should be low. However, to maintain a reasonable response time of the TAS, any dead volume between the sampling probe and the detection in the TAS should be minimized. Better still, the probe and the sensors should be integrated as much as possible, resulting in a true μ-TAS. Therefore, a silicon micromachined connector was designed and realized, as schematically shown in Figure 7. The funnel-like structure between the large opening surrounding the outer tube of the lumen and the V-shaped channel for the inner tube act as a guide for the insertion of the inner tube. A dead volume remained of only 180 nl, being only a fraction of that of a conventional probe, which is ca. 1.5 μl. Thus, the lag time of the TAS, equipped with this micromachined probe, is considerably reduced. An array of five finished probes, ready for cutting apart is shown in Figure 8.

Now that the sensor can operate in a relatively clean sample, the possible fouling of the semi-permeable membrane should be addressed. On the one hand, the probe - and operational parameters- can be designed in such a way, that the recovery ratio, R, is very high, near 100%. Such a design could guarantee that R remains high, say > 95%, even after mild fouling of the membrane. On the other hand, there is more

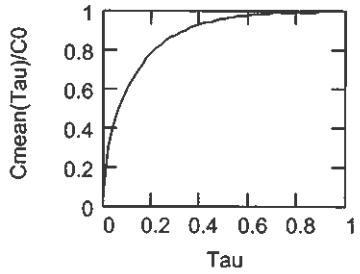

Figure 5a. Graph of the normalized mean concentration due to cylindrical diffusion as a function of the dimensionless variable, τ.

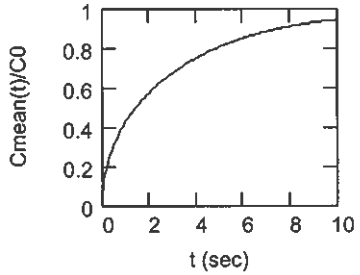

Figure 5b. Graph of the normalized mean concentration due to cylindrical diffusion as a function of time, t, for $D=1 \cdot 10^{-9}$ m^2/s and $R_0=150$ μm.

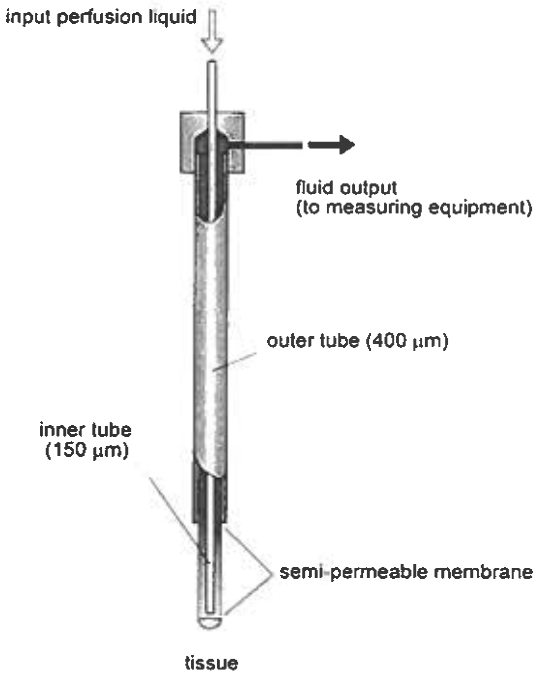

Figure 6. Impression of the double-lumen microdialysis probe. Reproduced with permission from reference [5]. Kluwer Academic Publisher, 1998.

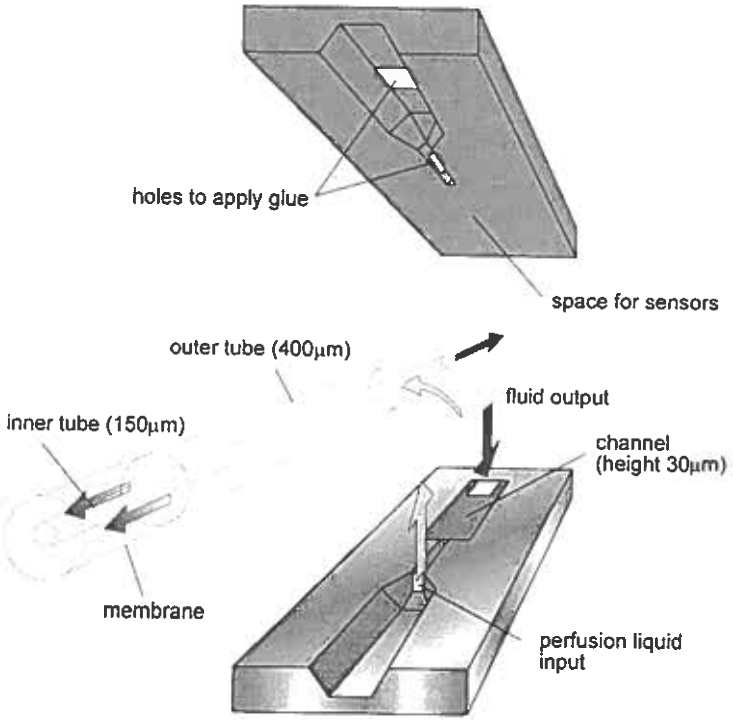

Figure 7. Exploded view of the microdialysis probe with connector. Reproduced with permission from reference [5]. Kluwer Academic Publisher, 1998.

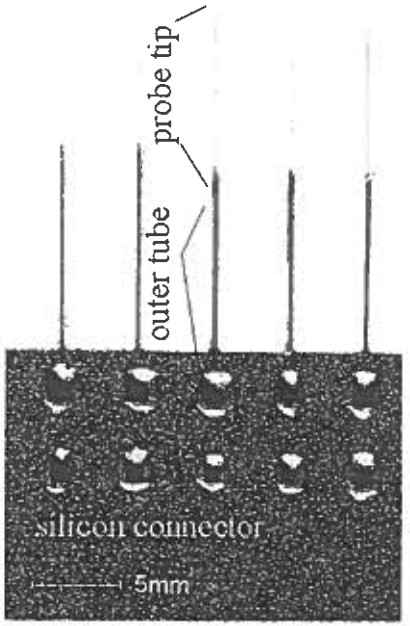

Figure 8. Realized Si-micromachined microdialysis probes. Reproduced with permission from reference [5]. Kluwer Academic Publisher, 1998.

freedom to chose a membrane that is less prone to fouling or better biocompatible than the material of the selector part of the sensor itself. In addition, the probe can be subjected to an overpressure of the perfusate with respect to the analyte, under the control of the TAS, thereby actively cleaning the membrane.

Calibration system

Although the sensor in the TAS as proposed in this chapter can operate in a relatively clean solution, due to the microdialysis probe as sample inlet, regular calibration of the sensor is still required. The system performing this calibration should of course preferably be a part of the TAS itself, as shown in Figure 2. For this purpose a dosing system is required, capable of dispensing calibration liquid in the carrier channel, leading to the sensor. The response to this plug of calibration liquid can be applied to determine the off-set and sensitivity of the sensor (i.e., if two reservoirs of calibration liquid are implemented). The system proposed in this chapter is based on the displacement of a fluid from a reservoir by the electrochemical production of gas bubbles *(6, 7)*.

In the realized structure, the calibration liquid to be dispensed is stored in a meander-shaped channel, starting in a reservoir filled with an electrolyte in which two electrodes are placed, as schematically shown in Figure 9.

By sending an electric current through the electrodes, gas bubbles are produced by the well-known anodic and cathodic electrolysis of water.

$$\begin{aligned} &\text{anode:} \quad 2H_2O(l) \rightarrow O_2(g) + 4H^+(aq) + 4e^- \\ &\text{cathode:} \quad 2H_2O(l) + 2e^- \rightarrow H_2(g) + 2OH^-(aq) \end{aligned} \tag{8}$$

These bubbles expand in the reservoir and drive out the calibration liquid, stored in the meander. After saturating the electrolyte with hydrogen and oxygen, the volume, V, of the gas bubbles and thus of the calibration plug can be precisely controlled according to

$$V = \frac{3i\Delta t}{4F} V_m \tag{9}$$

with i and Δt the amplitude and duration of the applied current pulse, respectively, F Faraday's constant, and V_m the molar gas volume at given temperature and (atmospheric) pressure.

The proposed system has been realized in Si micromachining technology and a photograph of the device, including two integrated electrochemical pumps and meander-shaped reservoirs for calibration liquid is shown in Figure 10 *(8)*. A detail of the pump, where the meander channels of the calibration units connect to the carrier channel, is shown in Figure 11. This figure clearly illustrates the precise design, possible by photolithographic techniques and silicon Deep Reactive Ion Etching. The calibration system is constructed of two layers. A bottom layer of silicon in which a channel structure is etched and a top layer of glass to create closed channels and to

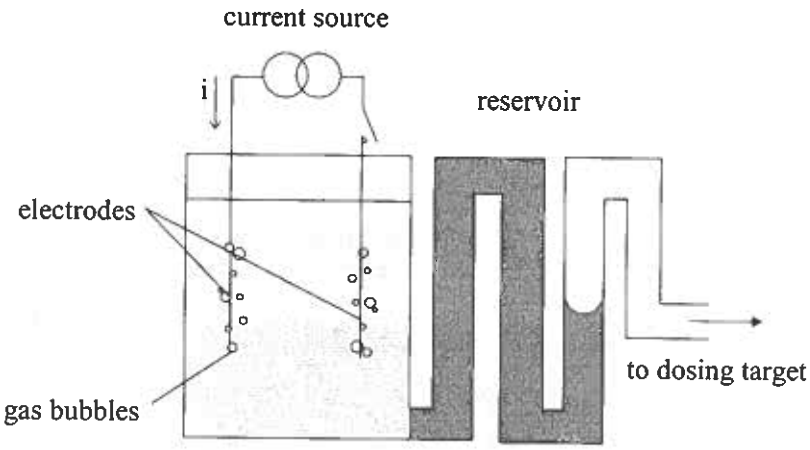

Figure 9. Principle of the proposed electrochemically actuated pump and dosing system. Reproduced with permission from reference [6]. Kluwer Academic Publisher, 1998.

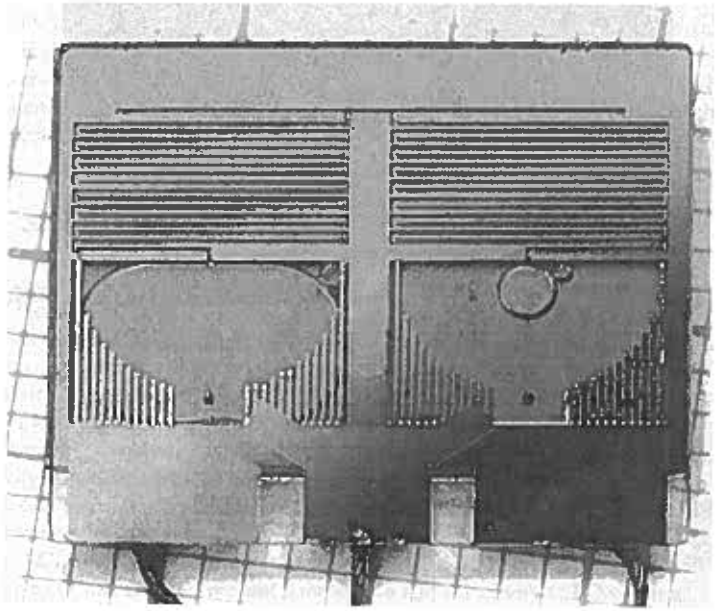

Figure 10. Photograph of the realized device, showing two complete calibration units.

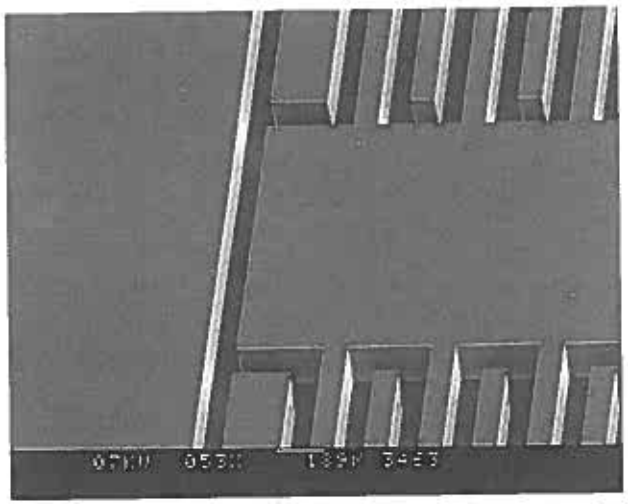

Figure 11. Photograph of a detail, showing the connection of the two meander-shaped channels to the carrier channel.

visually examine the flow through the channels. The electrodes for the electrolysis are deposited on the glass top layer.

A calibration system, capable of performing 20 calibration of 100 nl each, must contain 2 µl of calibration fluid. This 2 µl of calibration fluid is stored in the meander channel. A meander channel of 100 µm × 200 µm must therefore have a length of 10 cm. To push all the calibration fluid out of the meander channel, there must be at least 2 µl of electrolyte in the reservoirs. To have sufficiently electrolyte left for electrolysis when the 20th calibration is performed a reservoir volume of 5 µl is chosen.

A measurement setup is build to verify the calculated production of gas during electrolysis according to eq 9. A computer controlled current source (CCCS) is used for electrolysis. The current source is equipped with two current ranges, 0-100 µA and 0-2 mA. The connection holes of the reservoirs are sealed with epoxy (Araldit). The calibration system is then immersed in an electrolyte solution. The electrolyte consists of a 200 mM KNO_3 solution to which some detergent (Tween 20) is added. Using a vacuum system, air inside the calibration system is replaced by the electrolyte solution.

Using a CCD camera and a color monitor, as shown in Figure 12, the displacement of the fluid during electrolysis can be visualized. By measuring the displacement in combination with the channel cross-sectional area, the volume of the produced gas can be calculated. Precise dosing is shown to be possible in Figure 13, where the measured volumetric flow for Δt=5 s at the mentioned current values is shown, including the theoretical curve from eq 9.

To show an actual example of the calibration procedure of a pH-sensitive ISFET, the response of a two-point calibration on two injected calibration samples obtained with a system like the one described here is included in Figure 14.

Selection with an Electrolyte Conductivity (EC) sensor

One of the important sub-systems in any TAS is the detection. In many cases, optical techniques, such as luminescence, fluorescence or spectroscopy are applied, using full-size optical equipment. Only in a few cases, the optics, necessary for the detection, are integrated as well, which is a prerequisite for a real TAS *(9, 10)*. Considering size, electrochemical sensors seem to be better suited as detector in a TAS. Two regularly encountered types of sensors are amperometric and conductometric sensors *(11, 12)*. Due to their simple construction and the fact that selectivity is often already obtained in an earlier stage during separation, these sensors can give satisfying results. Better results, however, can possibly be obtained, when some selectivity is built-in in the detector. Although this seems to be impossible with an EC sensor, due to the inherently non-selective nature of EC, we will in the second part of this chapter, present a method to add selectivity to EC sensing.

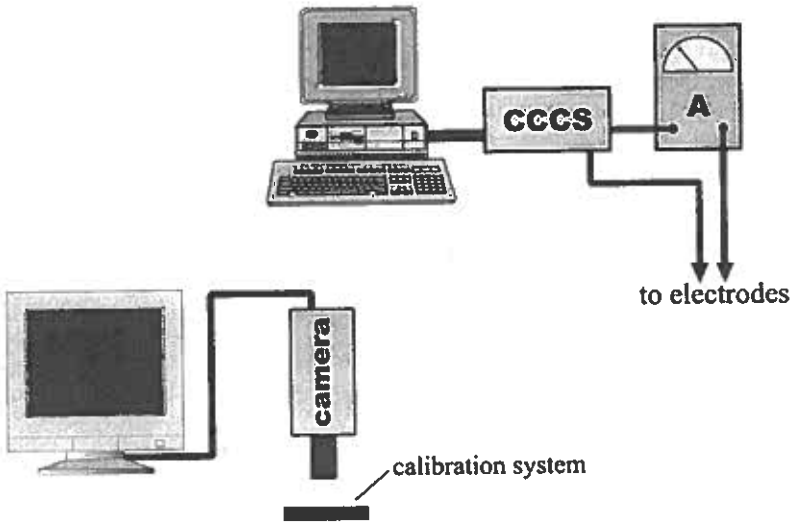

Figure 12. The measurement set-up, consisting of a computer controlled current source (cccs) to evoke gas bubbles by electrolysis and a ccd camera to monitor the fluid displacement.

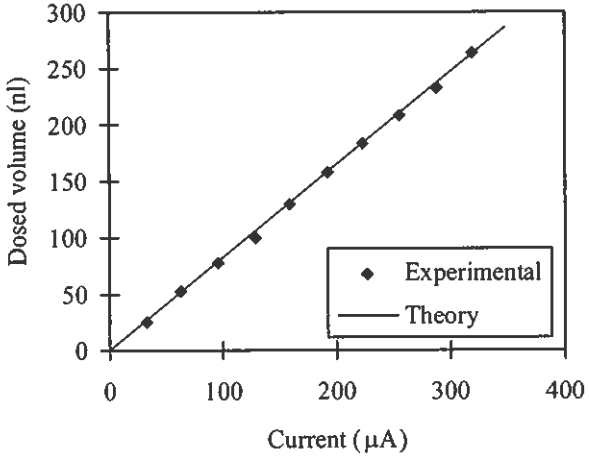

Figure 13. Measured dosed volumes after 5 s current actuation with given current amplitudes.

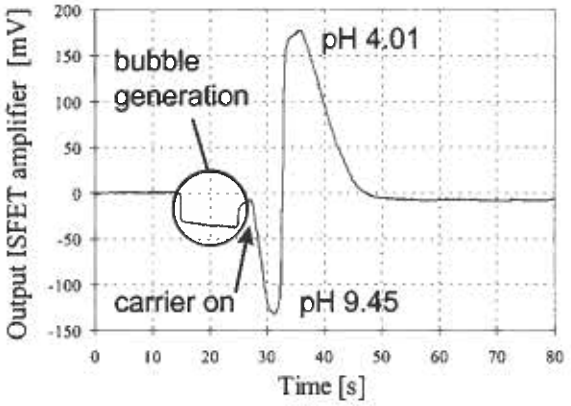

Figure 14. Measurement result of a two-points ISFET calibration downstream in the carrier flow. Reproduced with permission from reference [6]. Kluwer Academic Publisher, 1998.

Operational principle

A single EC measurement does not give any specific information on the ion concentrations that are present in the solution, when more than 2 types of ions are involved. However, a range of measurements at various temperatures of the electrolyte does, since the temperature dependence of the mobility of an ion is unique for that ion *(13, 14)*.

The total conductivity of an electrolyte expressed in terms of the limiting molar conductivities of the separate ions can be expressed by

$$\Lambda = \sum_{i=1}^{I} |z_i| c_i \lambda_i(T) \tag{10}$$

with z_i the charge of ion i, c_i the concentration, I the number of different types of ions and $\lambda_i(T)$ the limiting molar conductivity of ion i. This last factor is dependent on temperature and is specific for every single ion. The generalized polynomial fit of $\lambda_i(T)$ of order J with respect to temperature T_0 can be written as

$$\lambda_i(T) = \lambda_i^0 \sum_{j=0}^{J} k_{i,j} (T - T_0)^j . \tag{11}$$

with λ_i^0 the limiting molar conductivity for ion i at $T=T_0$. Since the coefficients $k_{i,j}$ are unique for ion i, the total conductivity Λ is a unique linear combination of the limiting molar conductivities $\lambda_i(T)$ with the specific ion concentrations as coefficients.

Using equations 10 and 11 the total conductivity of an electrolyte having I types of ions can now be calculated:

$$\Lambda(T) = \sum_{i=1}^{I} \left[|z_i| c_i \lambda_i^0 \sum_{j=0}^{J} k_{i,j} (T - T_0)^j \right] \tag{12}$$

Manipulation yields:

$$\Lambda(T) = \sum_{j=0}^{J} \left[(T - T_0)^j \sum_{i=0}^{I} \left(|z_i| c_i \lambda_i^0 k_{i,j} \right) \right] . \tag{13}$$

For conductivity measurements at N different temperatures, I types of ions and a polynomial fit of order J, a matrix equation can be formed using eq 13:

$$\begin{bmatrix} \Lambda_1 \\ \Lambda_2 \\ . \\ . \\ \Lambda_N \end{bmatrix} = \begin{bmatrix} 1 & (T_1 - T_0) & (T_1 - T_0)^2 & . & (T_1 - T_0)^J \\ 1 & (T_2 - T_0) & (T_2 - T_0)^2 & . & . \\ . & . & . & . & . \\ . & . & . & . & . \\ 1 & (T_N - T_0) & (T_N - T_0)^2 & . & (T_N - T_0)^J \end{bmatrix} \cdot \begin{bmatrix} k_{1,0} & k_{2,0} & . & k_{I,0} \\ k_{1,1} & k_{2,1} & . & . \\ . & . & . & . \\ k_{1,J} & k_{2,J} & . & k_{I,J} \end{bmatrix} \cdot \begin{bmatrix} |z_1| c_1 \lambda_1^0 \\ |z_2| c_2 \lambda_2^0 \\ . \\ |z_I| c_I \lambda_I^0 \end{bmatrix} \tag{14}$$

or

$$\overline{\Lambda} = \overline{\overline{T}} \cdot \overline{\overline{K}} \cdot \overline{c} . \tag{15}$$

The meaning of the terms is:

- $\overline{\Lambda}$ Vector containing measured conductivities at N different temperatures;
- $\overline{\overline{T}}$ Matrix with the temperature information;
- $\overline{\overline{K}}$ Matrix with the polynomial coefficients $k_{i,j}$;
- $\overline{c}$ Vector with the ion concentrations multiplied by the parameters $|z| \cdot \lambda_i^0$;

The question rises whether it is possible to calculate the vector $\overline{c}$ (containing the concentration information) from a known $\overline{\overline{T}}$ matrix and a measured $\overline{\Lambda}$ vector. When the $\overline{\overline{K}}$ matrix is assumed to be known, which implies a chosen set of ions, eq 14 can be written as

$$\begin{bmatrix} \Lambda_1 \\ \Lambda_2 \\ . \\ . \\ \Lambda_N \end{bmatrix} = \begin{bmatrix} \sum_{j=0}^{J} k_{1,j} (T_1 - T_0)^j & \sum_{j=0}^{J} k_{2,j} (T_1 - T_0)^j & . & \sum_{j=0}^{J} k_{I,j} (T_1 - T_0)^j \\ \sum_{j=0}^{J} k_{1,j} (T_2 - T_0)^j & \sum_{j=0}^{J} k_{2,j} (T_2 - T_0)^j & . & . \\ . & . & . & . \\ \sum_{j=0}^{J} k_{1,j} (T_N - T_0)^j & . & . & \sum_{j=0}^{J} k_{I,j} (T_N - T_0)^j \end{bmatrix} \cdot \begin{bmatrix} |z_1| c_1 \lambda_1^0 \\ |z_2| c_2 \lambda_2^0 \\ . \\ |z_I| c_I \lambda_I^0 \end{bmatrix} \tag{16}$$

where the $\overline{\overline{T}} \cdot \overline{\overline{K}}$ matrix is written as a single one. The elements in this matrix are polynomials for the n-th temperature (rows) and the i-th ion (columns). If the $\overline{\overline{T}} \cdot \overline{\overline{K}}$ matrix has an inverse, the concentrations will follow from

$$\overline{c} = \left(\overline{\overline{T}} \cdot \overline{\overline{K}} \right)^{-1} \cdot \overline{\Lambda} . \tag{17}$$

The first condition for having an inverse is that the matrix is square, so the minimal number of necessary experiments is equal to the number of ions to fit *(N = I)*. For $N > I$ an estimator must be used. The second condition is that the determinant is not equal to zero. This is true when the coefficients are different for every ion and the order of the polynomial is equal or larger than I - 1.

So, it is possible to find the concentrations of individual ions in a solution under the following conditions:

- The measured conductivity scan must be a linear combination of the temperature responses for the individual ions. This means that
  - → Every ion which is significantly present in the electrolyte conductivity must be represented in the calculations;
  - → No two ions may have the same temperature dependency (which will probably never be the case);
  - → When I types of ions have to be calculated, the conductivity of the electrolyte must be measured at least $N = I$ temperatures;

→ The order of the used polynomials is equal to or larger than the number of different ions to fit minus one ($J = I - 1$);

- The coefficients $k_{i,j}$ of the individual ions must be known. The coefficients for the third order fit are given by Harned and Owen *(15)* for nine types of ions;

Improvement by estimation

The calculation of ion concentrations using the basic algorithm of eq 17 requires conductivity measurements at as much as temperatures as the number of ions to be fitted. It is more accurate to do more measurements *(N > I)* and use an estimation method. In order to find the best fit from the measurements, some theory concerning parameter estimation is necessary. The method introduced here is a matrix based algorithm for minimizing the mean square error of the estimation *(16)*.

Consider the generalized system

$$\overline{\Lambda} = \overline{\overline{B}} \cdot \overline{c} + \overline{v} \qquad (18)$$

with

$\overline{\Lambda}$ the vector containing the observations,
$\overline{\overline{B}}$ a matrix representing the system (in our case equal to $\overline{\overline{T}} \cdot \overline{\overline{K}}$),
$\overline{c}$ the input vector to be estimated and
$\overline{v}$ the noise or error in the measurement.

The aim is to find an estimate $\hat{\overline{c}}$ for the vector $\overline{c}$ satisfying the observed vector $\overline{\Lambda}$. The theoretical description of this estimation is beyond the scope of this chapter. Under certain particular conditions a relatively simple estimation can be derived.

The linear minimum variance unbiased estimate $\hat{\overline{c}}$ of $\overline{c}$ given data $\overline{\Lambda}$ under these conditions is according to Gauss-Markoff theorem equal to

$$\hat{\overline{c}} = \left(\overline{\overline{B}}^T \overline{\overline{B}}\right)^{-1} \overline{\overline{B}}^T \cdot \overline{\Lambda} \qquad (19)$$

which reduces to eq 17 for a square matrix $\overline{\overline{B}}$. Because the variances σ_v^2 of the vector $\overline{v}$ are assumed to be equal, the moment matrix $\overline{\overline{C}}_{\overline{v}}$ can also be eliminated, and the error matrix can be expressed as

$$\overline{\overline{C}}_e = \left(\overline{\overline{B}}^T \overline{\overline{B}}\right)^{-1} \cdot \sigma_v^2 \qquad (20)$$

which contains all covariances of the fitted vector $\hat{\overline{c}}$ in its entries. So, the numbers on the diagonal of this error matrix are the variances of the fitted parameters. Using this knowledge, the standard deviation of the whole fit can be defined as

$$\sigma_c = \sqrt{\text{trace}\left(\overline{\overline{B}}^T \overline{\overline{B}}\right)^{-1}} \cdot \sigma_v \qquad (21)$$

where the trace function is the summing of the elements on the diagonal of a matrix.

Increasing the accuracy of estimation

Now the variance in the measurement error can be determined, the propagation of this error through the estimation algorithm can be evaluated. This was done for the situation where the number of applied temperatures is equal to the number of ions to be fitted *(N = I)*. However, by using more than *N* measurements, a decrease in the final error can be expected because of suppression of measurement noise.

In Figure 15 the normalized calculated standard deviation in the estimated concentration is represented for three different temperature ranges ($T_1..T_N$) and estimations for $N = 2$ to 11. For this numerical example, the coefficients $k_{i,j}$ for a 100 mM sodium chloride solution are used.

It can be seen that the accuracy of the estimation can be increased, either by increasing the number of measurements or the temperature range. The improvement in accuracy by increasing the temperature range is larger than the improvement obtained by using more measurements.

Summary

Reconsidering the original eq 16, describing the set of conductivity measurements at N temperatures, the ultimate method of determination should be

- Perform the measurements, by heating a solution while measuring the conductivity. Take more measurements (conductivities at known temperatures) than the number of ions to be fitted *(N > I)* since this will increase the accuracy of the estimation. Notice that the application of a large temperature sweep will increase the accuracy much more. Some conductivity meters have an automatic temperature compensation which must thus be switched off. Also the use of an auto range function will disturb the measurement since the variance in the measurement appeared to be constant per operational range;
- Assume a set of ions and calculate the matrix $\overline{\overline{B}}$ with the elements

$$\overline{\overline{B}}_{n,i} = \sum_{j=0}^{J} k_{i,j} \left(T_n - T_0\right)^j$$

with T_0 the reference temperature, T_n the temperature of measurement n, J the order of the polynomial fit and $k_{i,j}$ the polynomial fit coefficients for the temperature dependency of the mobilities (which can be found in literature *(15)*);
- Create the conductivity vector $\overline{\Lambda}$, which is a column of N conductivity measurements at N different temperatures;

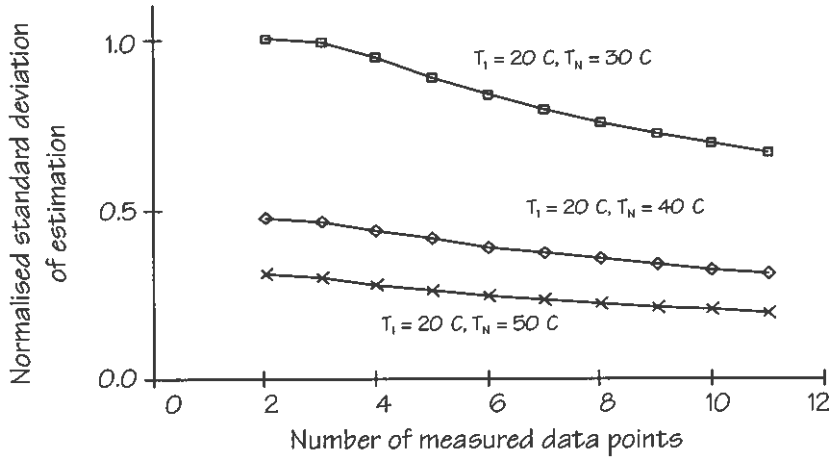

Figure 15. Effect of the temperature range, $T_I..T_N$, and the number of measurements on the estimation accuracy.

- Use eq 19 for finding the estimation vector $\hat{\bar{c}}$, which is a column of the $|z_i|c_i\lambda_i^0$products for the I ions. Because the charge of the ions z_i and the limiting molar conductivity λ_i^0 are known, the concentrations of the individual ions can be calculated.

The size of the error in the estimated concentrations is represented by eq 21 in terms of the covariance of the measurement error.

Improvement by implementing the zero charge condition

Because in practical solutions the total charge is equal to zero, the condition

$$\sum_{\text{Cations}} |z_i| c_i = \sum_{\text{Anions}} |z_i| c_i \qquad (22)$$

can be implemented in the algorithm in order to increase accuracy and to avoid useless answers like negative concentrations. This equation can be implemented in the model, eq 17, where the $\bar{\bar{T}} \cdot \bar{\bar{K}}$ matrix has now become the augmented $\bar{\bar{T}} \cdot \bar{\bar{K}}$ matrix. The elements in the augmented vector $\bar{\Lambda}$ and the augmented matrix $\bar{\bar{T}} \cdot \bar{\bar{K}}$ do not have an equal unity anymore. This does not make any difference for numerical evaluations, however.

This augmented model can be evaluated like the original model using the same estimation algorithm. However, the condition stated in eq 22 will have the same priority as every single measurement and so its importance will be suppressed with an increasing number of applied temperatures N. Two options are available for increasing its priority:

- The first option is to give the last row of the augmented $\bar{\bar{T}} \cdot \bar{\bar{K}}$ matrix a weight factor equal to the number of measurements.
- Another possibility is obtained by first reducing the measured information and then implementing the zero charge condition.

The further evaluation of these two options is treated elsewhere *(13)*. The error coefficient matrix of eq 20 has now become meaningless, and so the standard deviation of the fit (eq 21), since these are only valid when having equal variances $\bar{v}$ for all the measurements. The variances are not equal anymore, since the zero charge condition will have another variance than the actual conductivity measurements.

Implementation and results

The operational principle requires heating of the electrolyte. It is the benefit of a μ-TAS that local heating in a small measuring volume can be applied to rapidly heat the electrolyte locally. For this purpose, a dedicated EC-and-temperature sensor / thermal actuator was designed and developed *(17)*. The device is shown in Figure 16

and consists of a 1x1 mm^2 platinum structure on a glass substrate. A photograph of this device, mounted on a small piece of printed circuit board is shown in Figure 17. By applying an AC-current to one of the Pt-meanders, as shown at the left-hand part of Figure 16, the electrolyte can be heated locally. An increase of about 10^0C in temperature is obtained after a few milliseconds. Directly after switching off the heating current, both the EC and the local temperature are measured, as shown at the right-hand part of Figure 16: the structure now functions both as an interdigitated EC probe and resistive Pt-film temperature sensor.

From the measured results, a conductivity versus temperature plot can be constructed, as shown in Figure 18. After some calculations, using the theory described above, a unique fit can be obtained from which the specific ion concentrations can be calculated. A result, showing the successful application of the method is shown in Figure 19, in which the separate concentrations of 3 different ions in an electrolyte are determined. In a solution containing 25 mM NaCl, five different concentrations of KCl were added, as shown on the x-axis of Figure 19. The concentrations, as estimated by the algorithm are plotted on the y-axis and follow the added amount of KCl, whereas the estimated [Na^+] remains constant, as expected.

In conclusion, from a non-selective conductivity measurement, it is possible to find specific ion concentrations by recording the conductivity at different temperatures. The key to this is that every ion has its own specific limiting molar conductivity which depends uniquely on temperature. This method needs an assumed set of ions: the electrolyte conductivity is a linear combination of the specific ionic conductivities of these ions.

Additionally, every ion which is significantly present in the solution must be included in the calculation, since the method is based on the conductivity being a linear combination of all the separate ionic conductivities.

Summarizing, it can be said that the advantage of this method is that it introduces selectivity by smart data interpretation, and not by the sensor itself.

Concluding remarks

Research groups can continue to pursue the development of the ideal chemical sensor, or they can use the existing devices and micromachining techniques favorably in Total Analysis Systems. The flaws of existing detectors can thereby be circumvented. Amongst several other advantages, it is shown in this chapter, that μ-TAS's can offer a type of sample inlet, the microdialysis technique, which prevents severe fouling of the detector. Furthermore, it is shown that the function of calibration can be integrated in a μ-TAS by using electrochemically driven pumps.

Selection in EC sensing can be obtained by local heating, temperature- and EC-measuring. All these functions are shown to be performed with a device, comparably simple as an EC probe itself: properly shaped metal films. Only because of the small dimensions of a μ-TAS and the use of smart signal processing, the specific ion concentration determination by EC sensing is made possible.

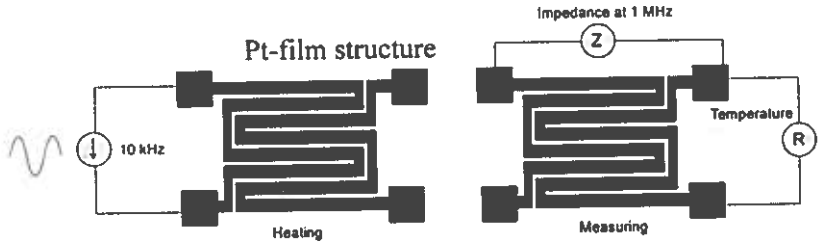

Figure 16. Integrated sensor-actuator device for local heating and temperature/conductivity measurement.

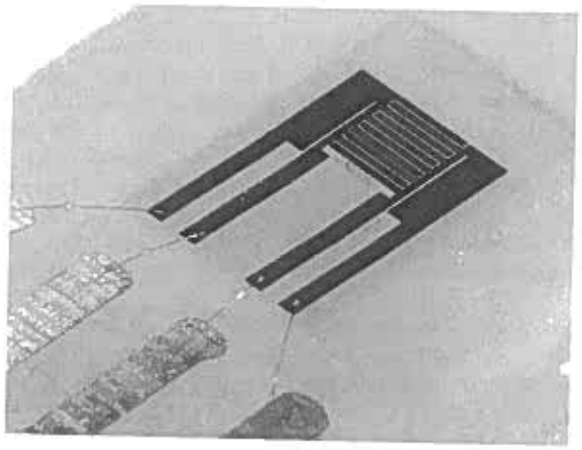

Figure 17. Photograph of the integrated sensor-actuator device on a glass substrate, mounted on a piece of PCB. The connection wires and strips are protected by transparent epoxy.

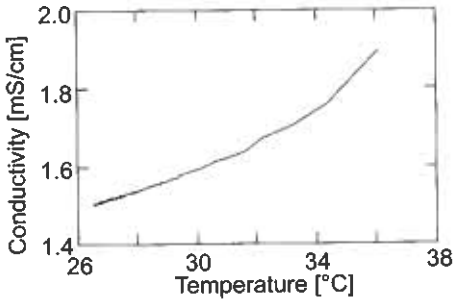

Figure 18. Measured conductivity versus temperature plot.

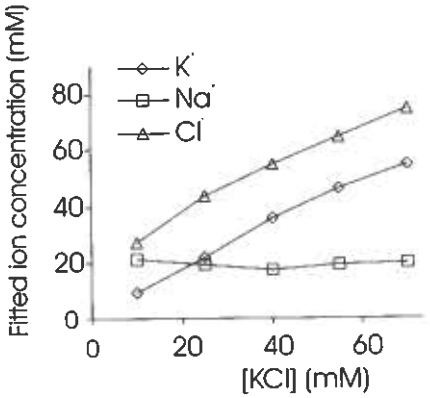

Figure 19. Fitted ion concentrations in five solutions with 25 mM NaCl and several KCl concentrations.

References

1. Manz, A.; Graber, N.; Widmer, H.M., *Sensors and Actuators* **1990**, *B1*, 244-248.
2. Manz, A.; Verpoorte, E.; Raymond, D.E.; Effenhauser, C.S.; Burggraf, N.; Widmer, H.M., In *Proc. μTAS '94;* van den Berg, A.; Bergveld, P., Eds.; Kluwer Academic Publ.: Dordrecht, 1995, 5-27.
3. de Boer, J.; Plijter-Groendijk, H.; Visser, K.R.; Mook, G.A.; Korf, J., *Eur. J. Appl. Physiol.*, **1994** *69*, 281-286.
4. Crank, J., *The mathematics of diffusion,* Oxford University Press: London, 1964.
5. Böhm, S.; Olthuis, W.; Bergveld, P., In *Proc. μTAS '98;* Harrison, D.J.; van den Berg, A., Eds.; Kluwer Academic Publ.: Dordrecht, 1998, 31-34.
6. Böhm, S.; Pijanowska, D.; Olthuis, W.; Bergveld, P., In *Proc. Dutch Sensor Conference*; van den Berg, A.; Bergveld, P., Eds; Kluwer Academic Publ.: Dordrecht, 1998, 91-95.
7. Bergveld, P.; Böhm, S.; Olthuis, W., International Patent Application, PCT/NL99/00057, 1999.
8. Böhm, S.; Olthuis, W.; Bergveld, P., *J. Biomed. Microdev.* **1999**, *1:2,* 121-130.
9. Leistiko, O.; Jensen, P.F., In *Proc. μTAS '98;* Harrison, D.J.; van den Berg, A., Eds.; Kluwer Academic Publ.: Dordrecht, 1998, 291-294.
10. Roulet, J.-C.; Fluri, K.; Verpoorte, E.; Völkel, R.; Herzig, H.-P.; de Rooij, N.F.; Dändliker, R., In *Proc. μTAS '98;* Harrison, D.J.; van den Berg, A., Eds.; Kluwer Academic Publ.: Dordrecht, 1998, 287-290.
11. Darling, R.B.; Yager, P.; Weigl, B.; Kriebel, J.; Mayes, K., In *Proc. μTAS '98;* Harrison, D.J.; van den Berg, A., Eds.; Kluwer Academic Publ.: Dordrecht, 1998, 105-108.
12. Fielden, P.R.; Baldock, S.J.; Goddard, N.J.; Pickering, L.W.; Prest, J.E.; Snook, R.D.; Treves Brown, B.J.; Vaireanu, D.I., In *Proc. μTAS '98;* Harrison, D.J.; van den Berg, A., Eds.; Kluwer Academic Publ.: Dordrecht, 1998, 323- 326.
13. Langereis, G.R., Ph.D thesis, University of Twente, Enschede, 1999.
14. Langereis, G.R.; Bergveld, P.; Olthuis, W., European Patent no. 98202690.8-2204, 1998.
15. Harned, S.; Owen, B., *The physical chemistry of electrolytic solutions*, Reinhold Publishing Corporation: New York, 1958.
16. Liebelt, P.B., *An introduction to optimal estimation*, Addison-Wesley Publishing Company: Reading, MA, 1967.
17. Langereis, G.R.; Bergveld, P.; Olthuis, W., *Sensors and Actuators* **1999**, *B 53/3*, 197-203.